Observation of the Full Exciton and Phonon Fine Structure in CdSe/CdS Dot-in-Rod Heteronanocrystals

Andrés Granados del Águila,[†] Bhawana Jha,[†] Francesca Pietra,[‡] Esther Groeneveld,[‡] Celso de Mello Donegá,[‡] Jan C. Maan,[†] Daniël Vanmaekelbergh,[‡] and Peter C. M. Christianen[†,*]

[†]High Field Magnet Laboratory, Institute for Molecules and Materials, Radboud University Nijmegen, Toernooiveld 7, 6525 ED Nijmegen, The Netherlands, and [‡]Condensed Matter and Interfaces, Debye Institute for Nanomaterials Science, Princetonplein 1, 3584 CC Utrecht, The Netherlands. C.d.M.D., D.V. and P.C.M.C. initiated the project. F.P. and E.G. synthesized and characterized the nanocrystals. F. P. fabricated and characterized the self-assembled samples. A.G.d.A., B.J. and P. C.M.C. planned the optical experiments. A.G.d.A. and B.J. performed the optical experiments and analyzed the results. A.G.d.A. and P.C.M.C. interpreted the data and wrote the manuscript. All authors intensively discussed the results and commented on the manuscript.

ABSTRACT Light emission of semiconductor nanocrystals is a complex process, depending on many factors, among which are the quantum mechanical size confinement of excitons (coupled electron–hole pairs) and the influence of confined phonon modes and the nanocrystal surface. Despite years of research, the nature of nanocrystal emission at low temperatures is still under debate. Here we unravel the different optical recombination pathways of CdSe/CdS dot-in-rod systems that show an unprecedented number of narrow emission lines upon resonant laser excitation. By using self-assembled, vertically aligned rods and application of crystallographically oriented high magnetic fields, the origin of all these peaks is established. We observe a clear signature of an acoustic-phonon assisted transition, separated from the zero-phonon emission and optical-phonon replica, proving that nanocrystal light emission results from an intricate interplay between bright (optically allowed) and dark (optically forbidden) exciton states, coupled to both acoustic and optical phonon modes.

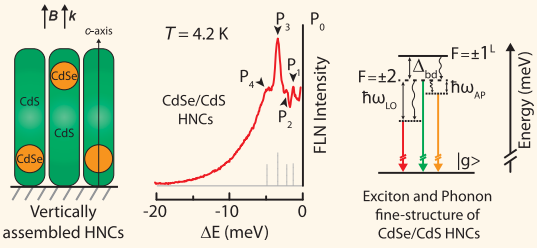

KEYWORDS: nanocrystals · excitons · acoustic phonons · optical phonons · core–shell heterostructure · fluorescence line-narrowing · magnetic fields

Colloidal semiconductor nanocrystals (NCs) are organically capped nanoparticles with optical properties that are dramatically different from those of the bulk semiconductor material. They exhibit very efficient light emission that can be tuned in wavelength by varying their size, composition and shape, making them suitable for optoelectronic and photonic applications.[1] The tunability stems from the quantum mechanical confinement of charge carriers leading to atomic-like, discrete energy levels resulting in size-dependent optical transitions due to electron–hole (exciton) recombination. In quasi-spherical wurtzite quantum dots (QDs) the electron–hole (e–h) exchange interaction and the intrinsic crystal/shape anisotropy lift the spin degeneracy of the exciton levels. As a result the lowest-energy exciton level is optically passive (the so-called dark state), just below an exciton state that is optically active (the bright state). The energy separation Δ_{bd} between the bright and dark exciton states scales with the exchange interaction as $\sim 1/R^3$, with R the NC radius.[2,3]

The sensitivity of the excitonic energy spectrum to the e–h exchange interaction gives rise to an extra degree of freedom to tailor the properties of NCs. The use of core–shell heteronanostructures (HNCs) that combine two semiconductor materials with different bandgap values permits to modify the e–h overlap.[4] Proper design of the alignment of the conduction and valence bands at the core–shell interface allows for the separate engineering of the spatial extensions of the electron and hole wave functions. In type-I heterostructures both electrons and holes are confined to the core (high e–h overlap), whereas in type-II heterostructures the electrons and holes are spatially separated (indirect excitons), lowering the e–h overlap. Recently also the

* Address correspondence to p.christianen@science.ru.nl.

Received for review February 20, 2014 and accepted May 26, 2014.

Published online May 26, 2014
10.1021/nn501026t

intermediate case (type-I$^{1/2}$ or quasi-type-II) has been realized, where one type of carrier is confined to the core, whereas the other type of carrier is delocalized over the core−shell. It has been shown that not only the radiative lifetimes[4−11] and the emission energies[4−7,9−12] depend on the e−h overlap, but that also the hot carrier relaxation,[13] the spin relaxation[14] and the strength of the quantum-confined Stark effect[15,16] are affected.

Despite the extensive knowledge on the exciton fine-structure in NCs and the corresponding optical properties, the precise photoluminescence (PL) recombination pathways are not entirely understood, in particular in the low-temperature limit. It is well established that the PL decay times of type-I CdSe QDs depend significantly on temperature T, being relatively short at room temperature (~10 ns) and much longer (~1 μs) at low temperatures.[3,17−19] This dependence is in qualitative agreement with the simple bright-dark exciton level diagram. At high temperatures PL emission originates from the higher-lying bright exciton state (short decay times), but when the thermal energy (k_BT) is smaller than Δ_{bd} the decay time increases.[17] This typical temperature dependence is absent for type-II CdSe/CdS HNCs, where the reduced e−h overlap leads to a vanishing Δ_{bd}.[8] However, in both cases quantitative agreement is lacking. Fitting the T-dependent lifetimes of CdSe QDs resulted in Δ_{bd}-values that are significantly smaller than those calculated by the effective-mass model[2,17] and those measured by fluorescence-line-narrowing (FLN) experiments.[20−22] Quantitative agreement of the T-dependent QD exciton lifetimes has been obtained using a model in which the exciton recombination is governed by optical transitions mediated by confined acoustic phonons. This model is supported by experimental results on QDs from different materials (CdSe, CdTe, PbSe and InAs).[23]

A second discrepancy between experiments and the simple bright-dark exciton model is the finite lifetime of the dark exciton state. With lowering temperature the exciton lifetime increases until it reaches a constant (plateau) value below 4.2 K. The actual value of this lifetime (~1 μs) is relatively short for a spin forbidden transition, as compared for example to triplet phosphorescence emission from organic chromophores (~1 ms). This apparent brightness has been attributed to phonon-assisted transitions[24] or due to mixing of the dark and bright exciton states, for instance as a result of unpassivated surface sites[25,26] or acoustic phonon excitations.[23]

Here we report the detailed investigation of CdSe dots that are embedded in a rod-like CdS shell (dot-in-rod HNCs). Such nanostructures can be fabricated with high monodispersity[27,28] and a small number of defects, leading to a high PL quantum efficiency.[9,11,15,16,29,30] Considering the type-I band alignment configuration of the conduction- and valence bands of bulk CdSe and CdS,[31,32] CdSe/CdS dot-in-rods are expected to be in the quasi-type-II regime, where the hole is confined to the core, whereas the electron wave function also extends to the shell (Figure 1(a)).[4,8,9,11] We employ FLN spectroscopy, using resonant excitation to select a subsection of HNCs out of the inhomogeneously broadened ensemble, whose bright exciton level matches the laser energy. This results in a large number of emission peaks with very narrow line widths <1 meV, approaching those of a single-dot experiment. Some of these transitions are demonstrated to originate from resonant Raman scattering processes, evidencing the ultrahigh structural quality of CdSe/CdS dot-in-rod HNCs. All transitions are identified by measuring their spectral position as a function of HNC size and magnetic field strength up to 30 T. In these experiments we used samples in which the rods form well-defined arrays with the long rod axis (the wurtzite c-axis) parallel to the excitation laser and the PL emission (Figure 1(c)).[33] Since the magnetic response strongly depends on the relative orientations of the c-axis and the magnetic field (B), the use of those self-assembled samples is crucial to fully elucidate the NC optical properties. We observe an unusual narrow zero-phonon emission transition, and apart of the regular optical phonon replicas, we resolve distinct acoustic phonon assisted emission, which provides direct experimental evidence that acoustic phonon excitations are

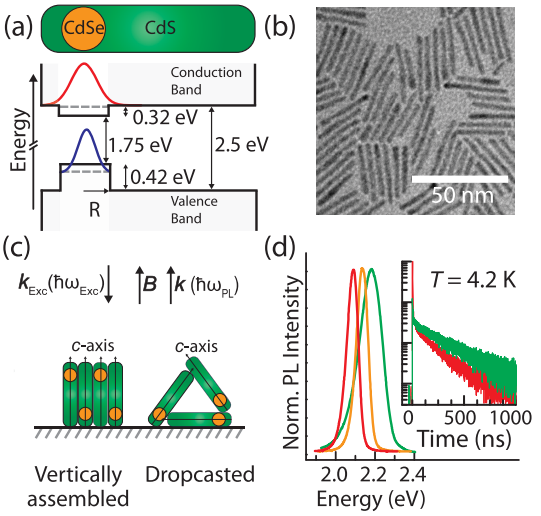

Figure 1. (a) Schematic representation of CdSe/CdS dot-in-rod HNCs. The bulk bandgap and band-offset values of CdSe and CdS with a type-I band alignment are indicated, leading to a quasi-type-II band alignment for dot-in-rod HNCs, where the hole wave function (blue solid curve) is confined to the CdSe core and the electron wave function (red solid curve) extends into the CdS shell. (b) Representative transmission electron microscope image of the CdSe/CdS LR sample (c) Schematic representation of a vertical rod assembly, where the rod c-axes are oriented parallel to the direction of the laser excitation (k_{Exc}, $\hbar\omega_{Exc} = P_0$ is the excitation energy), the PL emission (k, $\hbar\omega_{PL}$ is the energy of the emitted photoluminescence) and the applied field (B) (Faraday geometry). The dropcasted samples exhibit a more random orientation of their c-axes with respect to B and k. (d) PL spectra at 4.2 K of reference CdSe QDs (green curve), short HNCs (SRs, orange curve) and long HNCs (LRs, red curve). Inset: PL-decay curves for QDs (green curve) and LRs (red curve) on a semilog scale.

involved in the low-temperature radiative recombination of dark excitons within NCs. The e−h exchange energy is found to be reduced relative to a CdSe QD due to the extension of the electronic wave function into the shell (quasi-type-II), but the overall symmetry of the exciton is found to be spherical and not rod-like.

RESULTS AND DISCUSSION

Sample Characterization and Optical Properties. Dot-in-rod HNCs were prepared using the seeded growth methodology.[4] Spherical CdSe cores of fixed radius R = 1.6 nm were embedded in rod-like CdS shells. All samples were extensively characterized by transmission electron microscopy (Figure 1(b)) (see Methods section, Supporting Information Figure S1 and ref 33). Two different rod lengths were used: short rods (SRs) with length $L = (13.9 \pm 1.3)$ nm and diameter $D = (4.4 \pm 0.4)$ nm (aspect ratio AR = 3) and long rods (LRs) with $L = (39.8 \pm 1.7)$ nm and $D = (4.3 \pm 0.5)$ nm (AR = 9). The CdSe core is preferentially located at one end of the shell with its wurtzite c-axis parallel to the long rod axis (Figure 1(a,b)).[33] For the optical experiments ensemble samples were prepared using the procedure described in ref 34, which results in well-defined *self-assembled*, multilayer HNC arrays with their long rod axes parallel to the normal of the silicon oxide substrate (Figure 1(c)).[27,28,33] Also regular drop-casted samples were prepared in which the HNCs are more randomly oriented. For comparison a set of reference organically capped quasi-spherical CdSe QDs with R = 1.65 nm, 1.75 nm, 1.85 nm, 2.15 and 2.5 nm was prepared.

The CdSe/CdS HNCs exhibit PL emission in the visible range (Figure 1(d)) at a spectral position corresponding to carrier recombination from the CdSe core. The HNC PL is red-shifted relative to the reference QD with R =1.65 nm and the shift increases with AR together with a decreasing full width half-maximum (fwhm), changing from ∼140 meV for the QDs to ∼70 meV for the LRs. The low-temperature PL decay transients of both LRs and QDs (inset Figure 1(d)) show a similar biexponential decay with a fast and a slow component. The fast (∼10 ns) decay is ascribed to a transient emission from higher-energy exciton states prior to relaxation into the lowest-energy exciton level. The slow decay time, typically on the ∼ μs scale, reflects the radiative recombination lifetime of long-lived excitons emitted from the lowest-energy dark exciton level.

Fluorescence Line-Narrowing. In FLN experiments ensemble NC samples are resonantly excited at the red-edge of their lowest-energy absorption feature, which leads to the selective excitation of only a small fraction of the NCs whose energy gap matches the laser energy (P_0). This drastically reduces the inhomogeneous broadening of the optical spectra, resulting in an emission spectrum that consists of narrow lines and reveals the fine-structure of the exciton levels. The FLN spectrum of the reference CdSe QDs (lower panel Figure 2(a), green curve) shows a typical spectrum, which is usually explained in terms of the exciton energy scheme presented in Figure 2(b), where the levels are labeled by their spin projection F along the wurtzite c-axis. Photoexcitation occurs in the $F = \pm 1^L$ bright exciton level, followed by relaxation to the $F = \pm 2$ dark state from where radiative recombination occurs, leading to a zero-phonon line (ZPL) just below the excitation energy P_0. The resonant-Stokes shift (P_0-ZPL splitting) is given by the bright-dark splitting (Δ_{bd}). The ZPL is accompanied by phonon-assisted recombination at n = 1, 2 times ∼25−26 meV[35] below the ZPL, corresponding to the longitudinal optical phonon mode of CdSe (nLO$_{CdSe}$, in agreement with earlier reports[3,22,24]).

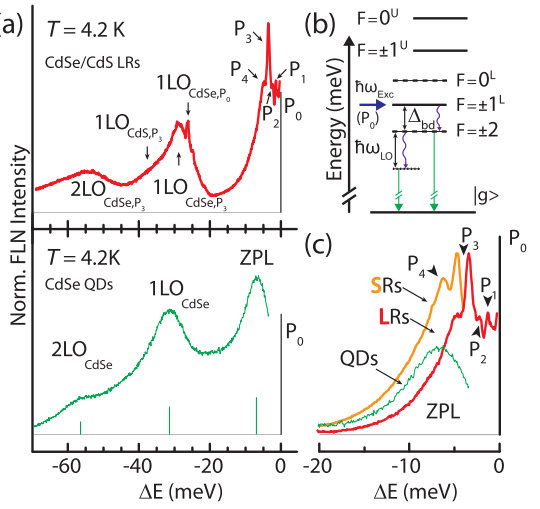

Figure 2. (a) FLN spectra at 4.2 K of LRs (upper panel) at excitation energy P_0 = 2.1382 eV and CdSe QDs with P_0 = 2.1778 eV (lower panel), revealing the exciton fine-structure. The energy scales are relative to the excitation energy P_0. The emission lines of the CdSe QDs originate from zero-phonon (ZPL) transitions and optical phonon (LO) replicas. The dot-in-rod HNCs exhibit a multitude of narrow emission lines, which are discussed in the main text. (b) Energy level scheme of the exciton fine-structure for wurtzite QDs. The levels are labeled in terms of the projection of the angular momentum F onto the c-axis (see text). Solid (dashed) lines correspond to bright (dark) exciton levels, responsible for optical transitions (solid green arrows) to the ground state $|g\rangle$. $\hbar\omega_{LO}$ corresponds to the LO phonon energy. The bright-dark exciton splitting (Δ_{bd}) is the energy difference between the $F = \pm 1^L$ and $F = \pm 2$ levels. Wavy arrows reflect non-radiative relaxation processes. (c) Comparison of the P_{1-4} emission lines within the FLN spectra at 4.2 K of LRs (red curve, P_0 = 2.1382 eV), SRs (orange curve, P_0 = 2.1977 eV) with the ZPL emission of a reference CdSe QD (green curve, P_0 = 2.1778 eV).

The FLN spectrum of the CdSe/CdS dot-in-rods (upper panel Figure 2(a), red curve) is roughly similar to that of the core-only QDs, but shows an unprecedented level of detail in both the ZPL and LO phonon replica regions. Most strikingly, in the ZPL region we resolve four narrow peaks just below P_0, labeled P_1, P_2, P_3 and P_4 (Figure 2(c)). P_1 and P_2 have a resolution-limited fwhm of ∼0.3 meV. The main peak in this region is the P_3 line, about 4 meV below P_0 with a fwhm of ∼0.7 meV. P_4 is less intense and broader (fwhm ∼1−1.5 meV). Also in the

phonon replica region we observe more lines than normally, resolving the usual CdSe phonon replicas ($1LO_{CdSe,P_3}$, $2LO_{CdSe,P_3}$), but also a shoulder at lower energy of $1LO_{CdSe,P_3}$ corresponding to the LO phonon mode of the CdS shell ($1LO_{CdS,P_3}$, 35 meV).[36] Surprisingly, we detect some very sharp lines (fwhm ~0.3 meV) on top of the 1LO phonon replica, of which the strongest is 26.4 meV below P_0 ($1LO_{CdSe,P_0}$). All of these peaks are labeled according to the phonon mode (*n*LO), the material (CdSe, CdS) and the peak from which they originate (P_0, P_3), as follows from the peak identification described below, using the behavior of the peaks as a function of excitation energy and magnetic field.

Dependence on Excitation Energy. To unravel the origin of all peaks in the FLN spectrum we have varied the excitation energy P_0 across the ensemble absorbance peak. Essentially, with increasing laser energy the size of the NCs that absorb the laser radiation becomes smaller, because the confinement energy increases with decreasing *R*. Figure 3(a) shows typical FLN spectra of HNC samples for three excitations energies, where the energy scale is taken relative to P_0 to permit direct comparison. We can distinguish two set of peaks. Peaks with positions that are (roughly) constant with varying excitation energy are indicated by the dotted lines (P_1, P_2, $1LO_{CdSe,P_0}$). In contrast, P_3, P_4, $1LO_{CdSe,P_3}$ and $1LO_{CdS,P_3}$ shift considerably with variation of the excitation energy (dashed lines). These two types of transitions are also visible in Figure 3(b), which shows the energy positions *versus* excitation energy of the main lines of the SR and LR samples.

Magnetic Field Dependence. A magnetic field has proven to be a powerful tool to characterize the nature of the optical transitions of colloidal dots and to identify the corresponding exciton states.[21,22,37] A magnetic field leads to a Zeeman splitting of the exciton energy levels, as well as mixing of their wave functions. Both effects strongly depend on the orientation of the NC *c*-axis with respect to the applied *B* and the observation direction *k* (see Figure 1(c)). Figure 4(a) shows the ZPL region of the 4.2 K FLN spectra of a self-assembled LR sample as a function of magnetic field *B*, using σ_+ polarized excitation at 2.1382 eV and detecting σ_- polarized photons. The zero-field spectrum consists of the four lines P_{1-4}. The P_1 and P_2 lines do not exhibit any shift with field (dashed brown and green lines). In contrast, the P_3 and P_4 transitions (dashed orange and red lines) exhibit a considerable shift down in energy with increasing field, which indicates the Zeeman splitting of the underlying exciton levels. In particular the P_3 line shows an interesting behavior at relative low fields below 10 T, which has not been observed previously and which is enlarged in Figure 4(c). At first, its spectral position is roughly constant, until at approximately 5 T the emission line splits into two. With increasing field the lower energy line becomes brighter at the expense of the higher energy peak, until above

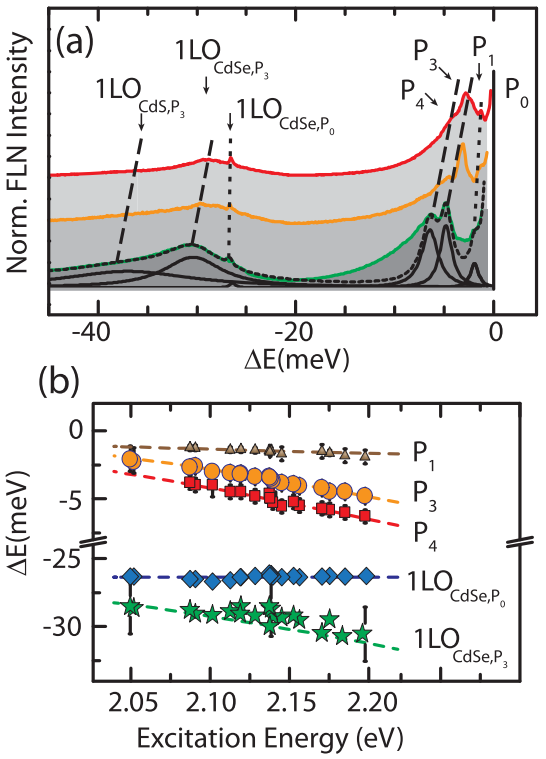

Figure 3. (a) FLN spectra at 4.2 K for CdSe/CdS LRs at excitation energies P_0 = 2.0872 eV (red curve) and 2.1126 eV (orange curve) and for SRs with P_0 = 2.1977 eV (green curve). The energy scale ΔE is relative to P_0. The spectra are vertically shifted for clarity. Black dashed-lines indicate transitions that shift with P_0. Dotted-lines indicate peaks that are roughly fixed in energy with varying P_0. The black dashed-line spectrum is a fitting curve of the bottom curve consisting of Lorentzian-shaped components (black solid lines). The integrated areas of the individual peaks, shown as percentages of the total detected PL intensity are I_{P_3} = 7.6, I_{P_4} = 9.8, $I_{1LO_{CdSe,P3}}$ = 18.5 and $I_{1LO_{CdS,P3}}$ = 20.7. (b) Evolution of the observed peak energies (relative to P_0) as a function of excitation energy for the main optical transitions of both LR and SR samples. The dashed-lines are guides to the eye.

10 T only the lower energy peak remains and gains intensity while shifting to lower energy with increasing field. At ~8 T we observe the appearance of an additional peak at an energy in between P_0 and P_3, labeled by SF_{P_0} and indicated by blue dashed lines in Figures 4(a,c). This line shows a rapid shift to lower energy with magnetic field.

An overall similar magnetic field behavior was found for dropcasted samples of the LRs (Figure 4(b,d)). However, the relative intensities of the peaks and their precise shifts with field strength differ, as a result of the more random orientation of the rods, as compared to the vertically aligned rods in the self-assembled sample. A clear difference is seen around ~6 T (see enlarged spectra in Figure 4(d)), when the spectrum develops two clear narrow lines, labeled by SF_{P_3} (orange dashed-line) and SF_{P_0} (blue dashed-line). At a field of about 15 T both features merge into one single peak, dominated by the SF_{P_0} transition, which becomes the most intense peak at high fields, even brighter than the P_3 line. These observations

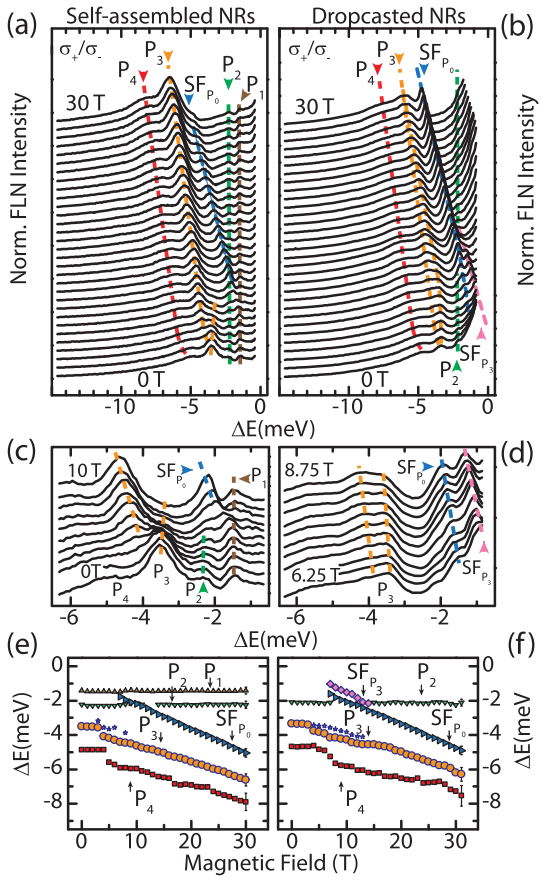

Figure 4. FLN spectra of self-assembled (a) and dropcasted (b) CdSe/CdS LRs as a function of magnetic field at 4.2 K. The spectra are plotted in 1 T steps and are vertically shifted for clarity. All spectra were recorded using σ^+ excitation at 2.1382 eV and σ^- detection. The evolution of P_1, P_2, P_3 and P_4 is guided by the dashed brown, green, orange and red lines, respectively. Spin-flip transitions SF_{P_0} (SF_{P_3}) are guided by blue (pink) lines. (c) Enlarged spectra of self-assembled LRs in the 0−10 T region. (d) Enlarged spectra of dropcasted LRs in the 6.25−8.75 T region. (e) and (f) show the energy of the most prominent transitions as a function of magnetic field for self-assembled and dropcasted rods, respectively.

are summarized in Figure 4(e,f), where we plot the relative spectral shifts as a function of applied magnetic field.

Spin-Flip Transitions. Application of a magnetic field leads to the appearance of extra peaks in the FLN spectrum, SF_{P_0} and SF_{P_3}, which shift relatively rapidly to lower energies with field. The SF_{P_0} peak is observed in both the self-assembled and the dropcasted samples and is attributed to a spin-flip (SF) process, originating from photoexcitation into the upper level of the Zeeman split $F = 1^L$ level and subsequent relaxation and recombination from its lower $F = -1^L$ Zeeman component (Figure 2(b)).[21,22] At zero field this transition is absent, whereas at high fields, the SF_{P_0} peak evolves linearly with increasing field (Figure 4(e,f)), corresponding to a Zeeman splitting of the bright $F = \pm 1^L$ exciton level characterized by a g-factor of ∼(2.5 ± 0.1) for self-assembled and ∼(2.3 ± 0.1) for dropcasted HNCs. Interestingly, the SF_{P_0} peak does not extrapolate to a zero shift at $B = 0$ (Figure 4(e,f)), which points to a finite energy splitting of the bright exciton level at zero field, in agreement with previous FLN experiments on CdSe QDs.[21] This zero-field splitting of the bright exciton state is attributed to a extra exchange interaction splitting due to an anisotropy in the plane perpendicular to the *c*-axis of the QDs.[38,39] In our case this anisotropic exchange splitting Δ_{xy} ∼(0.8 ± 0.3) meV, well within the range of values previously found for spherical dots using single-dot spectroscopy and FLN experiments.[21,38]

Surprisingly, the FLN spectrum of the drop-casted sample shows an additional spin-flip transition SF_{P_3} in intermediate fields of 5−15 T, which has not been observed before. This line exhibits a linear *B*-dependence with a field shift that is faster than that of the SF_{P_0} line and that corresponds to a g-factor of ∼ (2.8 ± 0.1). Because of this higher g-factor, the SF_{P_3} line merges with the SF_{P_0} transition around 15 T, after which only one spin-flip transition remains. Furthermore, the field dependence of SF_{P_3} directly extrapolates to the *origin* at zero-field, indicating a degenerate level at zero field. We assign SF_{P_3} to the spin-flip of the dark exciton ($F = \pm 2$), after photoexcitation of a $F = +2$ exciton and recombination from a $F = -2$ exciton (Figure 2(b)). This is consistent with the absence of a zero-field splitting for this line because $\Delta_{xy} = 0$ for a dark state.[38,39] We are able to observe the spin-flip of the dark exciton because of the high resolution reached in our FLN experiment. This dark exciton spin-flip transition is only observed at finite fields in the drop-casted sample. At low fields the oscillator strength of the dark exciton levels is too low to absorb laser light. With increasing field the dark exciton acquires oscillator strength due to magnetic field induced mixing between bright and dark excitons, which occurs for HNCs whose *c*-axis makes an angle (θ) with the direction of the *B*-field.[2] For the same reason the PL decay time of spherical dots drastically reduces with field.[40,41] In contrast, when the *c*-axis is parallel to the *B*-field, like in the case of the self-assembled sample, exciton mixing does not occur and the dark exciton state remains dark at all fields, meaning that for this sample the SF_{P_3} transition is not observed. The differences in the bright exciton g-factor in both samples support this picture. The magnitude of the Zeeman splitting depends on the angle θ, being maximal for NCs parallel to the field direction (θ = 0, self-assembled sample) and zero for NCs perpendicular to *B*. For random NC orientation, like in the dropcasted sample, the Zeeman energy is averaged over all possible orientations, yielding a lower g-factor.

The actual values for the g-factors of the bright (2.3−2.5) and dark (2.8) excitons are in agreement with the results of previous magneto-FLN studies[21] and single-dot spectroscopy.[38,42] Together with the value of the anisotropic exchange splitting Δ_{xy} (∼0.8 meV) they define the full field dependence of all lowest energy exciton levels (Figure 5(c)).

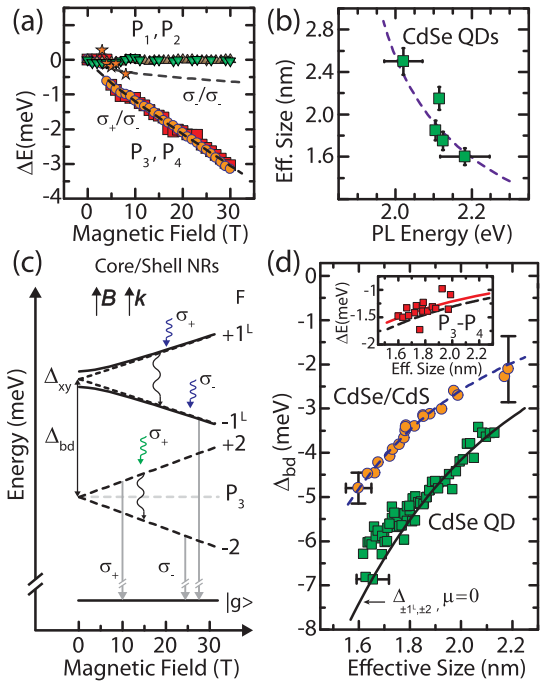

Figure 5. (a) Relative energy shift of the P_{1-4} lines with magnetic field. For easy comparison the zero field energy of each line has been subtracted. P_1 and P_2 (brown up-triangles and green down-triangles, respectively) do not depend on B as expected for a Raman scattering transition. P_3 and P_4 (orange circles and red squares, respectively) exhibit the same shift, consistent with the assignment of P_3 being the ZPL and P_4 its acoustic phonon replica. The dashed lines are calculated shifts given by the field dependence of the lowest lying excitons levels. (b) Determination of the effective exciton size as a function of the peak position of the nonresonant PL emission of CdSe QDs. The dashed curve is calculated using the tight-binding method.[36,56,57] (c) Field dependence of the $F = \pm 1^L$ and $F = \pm 2$ levels, determined from the measured g-factors and the zero-field splitting Δ_{xy} of $F = \pm 1^L$. Wavy arrows correspond to excitation processes. PL transitions to the ground state $|g\rangle$ are indicated by solid vertical arrows. The transitions are labeled by the preferential circular polarization ($\sigma^{+,-}$). Spin-flip transitions are labeled by black wavy arrows. (d) Δ_{bd} as a function of effective NC size for spherical NCs (green squares) and dot-in-rods (orange circles). The solid and dashed lines were calculated within the effective-mass-model.[2] Inset: size-dependence of the acoustic phonon energy (P_3−P_4) determined from the acoustic phonon replica observed in the FLN spectra (red squares). The red solid-line is the best fit to the data assuming a $\propto 1/R$ dependence. The black dashed line gives the size-dependence of the lowest-energy acoustic phonon breathing mode, with $l = 2$ and $m = 0$, of an isolated CdSe sphere obtained according to Lamb's theory.[44]

Zero-Phonon Line. The main peak (P_3) in the FLN spectrum is attributed to the zero phonon line, resulting from recombination of the $F = \pm 2$ dark state (Figure 2(b)). It has a narrow line width (fwhm ~0.7 meV) and its relatively high brightness suggests an intrinsic, nonzero, oscillator strength for the ground dark exciton. The energy shift relative to the laser excitation corresponds to the bright-dark splitting Δ_{bd}, which varies from 2 to 5 meV with increasing laser excitation energy (decreasing size) (Figure 3(b)). The full magnetic behavior of the (P_3) line (Figure 4(c)) can be readily understood within this picture. At low fields, when ($g\mu_B B < \Delta_{xy}$), all transitions from the $F = \pm 1^L$ to the $F = \pm 2$ levels might occur. In this field range the $F = \pm 1^L$ levels are mixed and linearly polarized. With increasing field $g\mu_B B > \Delta_{xy}$ the mixing of the bright exciton level disappears and at the same time the $F = +2$ dark exciton level depopulates due to its Zeeman shift to higher energy, leading to the redistribution of PL emission intensity from the higher energy component of P_3 to a lower energy component around 3 T. The higher energy component follows the energy separation of the $F = -1^L$ and $F = -2$ levels, whereas the lower energy component above 5 T follows the difference in energy of the $F = +1^L$ and $F = -2$ levels. This is shown by the dashed lines in Figure 5(a) calculated from the field-dependent exciton levels in Figure 5(c). This simple model is able to accurately reproduce the B evolution of the ZPL for the vertically aligned NRs, in the absence of field-dependent exciton mixing.

Optical Phonon Replicas. The FLN spectra show the regular, relatively broad, LO-phonon replicas (nLO_{CdSe,P_3}) at energies corresponding to 1 and 2 times the LO-phonon energy in CdSe, measured relative to the ZPL line P_3.[22,24] As expected, the LO-phonon replica peaks follow the ZPL line P_3, shifting to lower energy with increasing excitation energy (Figure 3(b)) and with increasing magnetic field strength,[22] shown in Supporting Information Figure S2. The dot-in-rod systems exhibit an additional signal around 35 meV below the ZPL line ($1LO_{CdS,P_3}$), which can be attributed to the LO-phonon replica of the CdS shell (see Figure 1(a), Figure 3(a) and Supporting Information Figure S3). This unambiguously proves that the dark exciton not only probes the CdSe core, but also the CdS shell, which is consistent with the electron wave function leaking out of the CdSe core,[8,9,11] giving a quasi-type-II exciton.

Acoustic Phonon-Assisted Transitions. Below the ZPL line P_3 we observe an additional peak P_4, which has a larger line width (fwhm ~1 meV). The energy separation between P_3 and P_4 is ~1.5 meV and is found to be constant as a function of magnetic field (Figure 5(a)). We identify this transition as an acoustic phonon (AP) replica of the ZPL, arising from the lowest energy breathing mode of CdSe.[23,43,44] This assignment is supported by the dependence of the $P_3 - P_4$ splitting on excitation energy, which is given by the size dependence of the acoustic phonon mode (see below). Confined acoustic phonon modes have been observed before in NCs by low-frequency Raman scattering,[45−48] ultrafast pump−probe spectroscopy[49−51] and spectral hole burning[52] experiments. However, direct experimental evidence on the role of these low-energy acoustic excitations in the *radiative recombination* of dark excitons is scarce.[43,53] The presence of the AP replica in our FLN emission spectra is, therefore, an important proof that acoustic phonons are involved in the radiative recombination of excitons in colloidal semiconductor nanocrystals. Generation of acoustic

phonons will elastically distort the NCs resulting in an additional mixing between bright and dark excitons, explaining the finite oscillator strength of the optically forbidden lowest exciton level.[23,54,55] This has important consequences for the temperature dependence of the PL decay times of semiconductor NCs. In a simple two-level model this *T*-dependence is governed by the energy separation Δ between the two emitting states at thermal equilibrium (Figure 2(b)). Fitting the *T*-dependent lifetimes of CdSe QDs resulted in Δ-values of about 1 meV, significantly smaller than the bright-dark splitting (Δ_{bd}) in the simple bright-dark exciton model.[17] Instead, the energy of the acoustic phonon mode found here agrees well with such a small activation energy, strongly suggesting that acoustic phonons play an important role in the recombination of NC.[23] We note, however, that the description of the full *T*-dependence of the PL decay times of ensemble NC distributions after nonresonant excitation should include all radiative decay channels. For instance, from the fitting curve in Figure 3(a), we estimate that the relative contribution of the ZPL-P_3 (*i.e.*, direct dark exciton recombination) (I_{ZPL} = 7.6%) and its first acoustic-phonon replica P_4 (I_{P_4} = 9.8%) is roughly ~20% of the low-*T* PL intensity. The main contribution (~40%) comes from the lowest 1LO phonon replicas, involving CdSe ($I_{1LO_{CdSe,P3}}$ = 18.5%) and CdS ($I_{1LO_{CdS,P3}}$ = 20.7%). The remaining intensity originates from the nonresonant signal just below P_4 and the higher order LO phonon replicas (not shown). The nontrivial intensity distribution over the different radiative decay paths provides the crucial insight that the optical emission of NCs is given by an intricate and complex interplay between excitons and phonons.

Raman Scattering. The FLN spectrum shows additional sharp lines in the region of the LO phonon resonance (*e.g.*, $1LO_{CdSe,P_0}$) and just below the laser energy (P_1 and P_2). All these transitions are characterized by (i) a Lorentzian-like line shape with a resolution-limited line width; (ii) a weak dependence on the laser excitation energy (NC size); and (iii) a constant intensity and energy position as a function of the applied magnetic field strength. We, therefore, attribute these lines to resonant Raman scattering: the shift of the $1LO_{CdSe,P_0}$ line, 26.4 meV below P_0, matches the LO phonon of CdSe. The shifts of P_1, P_2 (~1.5−2.5 meV below P_0) match the energies of typical acoustic phonon modes of CdSe. The shift of P_1 equals the $P_3 - P_4$ splitting, suggesting that the same acoustic phonon mode is involved. The detailed behavior of the Raman scattering peaks as a function of laser excitation energy, magnetic field strength and temperature will be described elsewhere. The observation of resolution-limited Raman modes of CdSe, together with the sharp exciton emission lines, indicates the extremely high structural quality of our dot-in-rod systems. Apparently, this system represents an almost ideal single-crystalline NC with a perfect core−shell interface in which the influence of surface traps can be neglected, leading to a high PL quantum efficiency and a narrow size distribution to give resolution-limited line widths in an ensemble measurement under resonant excitation.

Exciton and Phonon Fine-Structure. The unprecedented high quality of the FLN spectrum of our dot-in-rod NCs, exhibiting many well-resolved narrow peaks, each with a characteristic dependence on excitation energy and magnetic field strength, permits us to fully unravel all recombination pathways of the photoexcited excitons. It also allows to us to determine the size-dependence of important parameters, such as the e−h exchange interaction, the e−h overlap and the acoustic phonon energy. To determine the effective size of the exciton wave function we have measured the PL emission energies at 4.2 K of a set of reference CdSe QDs (Figure 5(b)). The PL energy increases with decreasing size, following the regular behavior of quantum confinement in a spherical dot. The dashed line in Figure 5(b) is calculated using an empirical tight-binding model that links the PL emission energy to the volume of the quantum dot and, therefore, to the effective volume of the exciton wave function.[36,56,57] We use this relationship to estimate the effective size of the exciton wave function in our dot-in-rod HNCs. Here we assume that the excitons in the dot-in-rod HNCs still have spherical symmetry, even though the electron- and hole wave functions are separated in real space (Figure 1(a)).[58] This assumption is justified by the magnetic field dependence of the exciton levels (Figure 5(c)), which clearly corresponds to a QD with spherical symmetry and not to a rod-like system, in which the lowest energy state would have $F = 0$.[59,60] Furthermore, as compared to other core−shell NC systems,[7] we observe a small red-shift of the PL emission of the dot-in-rod HNCs, relative to the reference spherical QDs (Figure 1(d)). We quantitatively describe this red-shift by a slight increase of the effective volume of the exciton wave function, due to a small leaking of the (electronic) wave function into the surrounding rod-like shell. The fact that we observe a small contribution of the phonon replica arising from the CdS LO phonon confirms that the exciton probes the rod-like CdS shell, but its relatively low intensity is consistent with a rather small leakage of the electron-wave function into the CdS shell. Within this spherical approximation, we can link the photon excitation energy P_0 of the FLN experiments directly to the effective size of the NCs. Figure 5(d) shows the Δ_{bd} energy of SR and LR samples (orange circles) and the set of reference spherical CdSe QDs (green squares) as a function of effective size.

The bright-dark splitting Δ_{bd} decreases with size for both systems. At each size Δ_{bd} of a dot-in-rod HNC is smaller than that of the corresponding QD. To explain this difference we model Δ_{bd} within the effective-mass-approximation (EMA) model of Efros.[2] For the spherical QDs we obtain excellent agreement (solid black line in Figure 5(d)) without any adjustable

parameters, using only literature values for CdSe: bulk exchange splitting $\hbar\omega_{ST} = 0.13$ meV, ratio of e/h mass $\beta = 0.28$, shape eccentricity $\mu_{shape} = 0$, anisotropy splitting $\Delta_{cf} = 25$ meV,[2] and exciton Bohr radius $a_B = 4.9$ nm.[56] Since the size dependence of Δ_{bd} is mainly determined by the exchange energy ($\eta_{core} \sim R^{-3}$),[3] the smaller Δ_{bd} of dot-in-rods points to a reduced e−h exchange interaction. The exchange coupling depends on the spatial overlap of the electron (ψ_e) and hole (ψ_h) wave functions and is directly proportional to the integral $\chi_{e-h} = \int |\psi_e(r)|^2 |\psi_h(r)|^2 \, dV$ over the NC volume. Spatial separation of electrons and holes leads to a diminished χ_{e-h} integral, hence a weaker exchange interaction. To quantify Δ_{bd} in the dot-in-rod HNCs, we define its exchange term as $\eta_{CS} = \theta_{e-h}\eta_{core}$ and θ_{e-h} a dimensionless parameter between 0 and 1, which accounts for the e−h spatial separation. This term arises from normalization of χ_{e-h}. We find good agreement with $\theta_{e-h} = 0.6$ as the only free parameter to model P_3-ZPL, as shown in Figure 5(d) by the blue dashed-line. Recent EMA calculations for CdSe/CdS QDs[8] have shown a linear dependence between the exchange splitting and the e−h overlap integral. Following this interpretation we conclude that the lowered value of θ_{e-h} proves a reduced e−h overlap in dot-in-rod HNCs.

The red squares in the inset of Figure 5(d) illustrate the size-dependence of the energy difference between the ZPL (P_3) and the acoustic phonon replica (P_4). This difference is equal to the energy of a confined acoustic mode excitation. This size-dependence can be fitted by $\hbar\omega = 2.45/R$ (red solid-line in the inset of Figure 5(d)). Such a $\propto 1/R$ dependence is typical for confined acoustic phonon modes in spherical nanoparticles,[61−63] as well as for radial breathing modes in rod-like nanostructures.[64−66]

In a first approximation, we compare the experimental data with the breathing modes of an *isolated* spherical CdSe QD, using Lamb's theory treating the NC as a vibrating, stress-free, homogeneous elastic body with spheroidal shape.[44,45,55,61,63] The acoustic oscillations of spherical nanoparticles have two types of solutions which are classified in torsional and spheroidal eigenmodes, whose angular frequencies ($\omega^{s,t}_{l,m}$) depend on the angular-momentum l and radial mode m numbers. The spheroidal frequencies depend on the ratio between longitudinal (c_l) and transversal (c_t) wave velocities in the medium. $c_t/c_l = 0.42$ (0.44) for CdSe (CdS) with $c_t = 1.504 \times 10^3$ m/s.[44,45] Using CdSe values, we find that the lowest-energy spheroidal mode (SM) of an isolated CdSe sphere, with $l = 2$ and $m = 0$, is in good agreement with the experimental data. The vibrational energy of that SM, $\hbar\omega^s_{2,0} = 2.46 c_t\hbar/R$, is depicted by the black dashed-line in the inset of Figure 5(d) (see also Supporting Information Figure S4 and Supporting Discussion). For spherical CdSe type-I QDs, coupling of the dark exciton to the acoustic phonon mode $l = 2$ has been proposed both theoretically and experimentally.[23,67]

We find good agreement between the experimentally determined energy of the AP mode and the simple model for confined modes in an *isolated spherical* QD. This is very remarkable because acoustically the dot-in-rod HNCs should behave as rod-like systems, since the elastic properties of CdSe and CdS are quite similar. However, calculation of the energies of the radial and extensional breathing modes of isotropic, elastic rods, within linear elasticity theory,[65,68] leads to values that are either too large (radial breathing modes) or too small (extensional breathing modes) (see Supporting Information Figure S5 and Supporting Discussion). A recent nonresonant Raman study has reported the observation of the radial breathing mode of CdSe nanorods, with a vibrational energy that depends only on the radius of the rod and not on the aspect ratio.[65] A typical radial breathing mode energy of ∼2.7 meV has been found for a rod with a 2 nm radius, which is close to the size of the outer CdS-shell in our samples. Indeed, this energy is too large to explain the energy of the AP mode in our CdSe/CdS dot-in-rod HNCs. However, we cannot exclude that such radial breathing mode exists in our data within the broad sideband just below the P4 peak in our FLN spectra (see Figure 3(a)). A possible explanation for the discrepancy is given by the different nature of the two experiments. In our work we determine the acoustic phonon energy as the difference in energy between the AP replica and the zero phonon emission(P_3-P_4) in the FLN spectrum. In this transition the exciton−phonon interaction plays a crucial role, where the spatial extension of the exciton wave function might set an additional boundary condition for the excitation of the phonon oscillation, which is absent in the case of a nonresonant Raman excitation of a regular rod-like system. In the CdSe/CdS systems studied here, the exciton wave function has a different (spherical) symmetry compared to the overall (rod-like) shape of the nanocrystal, which might lead to the excitation of acoustic phonons derived from the core. Further nonresonant Raman experiments in dot-in-rod HNCs and additional calculations of confined phonon modes in such systems may validate this scenario.

CONCLUSION

In conclusion, we have demonstrated that CdSe/CdS dot-in-rod HNCs provide a powerful model system to investigate the fundamental optical properties of semiconductor nanocrystals. Their shape allows to fabricate self-assembled arrays with a well-defined orientation of the NC crystallographic axis relative to external parameters, such as an applied magnetic field and the observation direction. The high structural quality of the CdSe/CdS HNCs is exemplified by the appearance of resonant Raman peaks and narrow fluorescence lines in an ensemble experiment under resonant excitation. The direct observation of

an acoustic phonon assisted transition, besides the sharp zero-phonon emission and optical phonon replicas, highlights the importance of vibrational modes for the exciton recombination of nanocrystals. The overall symmetry of the exciton wave function in the CdSe/CdS dot-in-rods has been proven to be spherical, although the HNCs display a quasi-type-II band alignment with a reduced electron–hole overlap and a smaller exchange energy.

METHODS

Sample Synthesis and Preparation of Self-Assembled Layers. The nearly spherical CdSe NCs were synthesized by hot injection of organometallic precursors into a coordinating solvent mixture, following methods reported by de Mello Donegá *et al.*[69] The CdSe QDs were dispersed in toluene and the solution was dropcasted on GaAs substrates. CdSe/CdS dot-in-rod HNCs were prepared using the seeded growth methodology[4] following an adaptation of the method reported by Carbone *et al.*[28] (see Supporting Information Methods and ref 33). CdSe/CdS dot-in-rod HNC samples were prepared in two different geometrical configurations with respect to the deposition substrate: (i) randomly oriented where HNC/toluene solutions were dropcasted on a Si/SiO_2 substrate to give a randomly oriented sample, and (ii) vertically oriented (with the long rod axes parallel to the normal of the substrate). Here, following the method described by Zanella *et al.*,[34] ensembles of self-assembled HNCs vertically aligned were prepared by depositing a highly concentrated HNC/dichlorobenzene solution (~2 μM concentration) on a 10×10 mm^2 Si/SiO_2 substrate. The solvent evaporation rate was kept very slow in a solvent saturated atmosphere to ensure the formation of predominately upstanding HNC assemblies. The preferential orientation of the HNCs in the assembly was studied by X-ray diffraction.

Optical Measurements. Optical experiments at low temperatures and high magnetic fields were performed on a set of NC ensemble samples, using three spectroscopic techniques: photoluminescence (PL), time-resolved PL (TRPL) and fluorescence line narrowing (FLN) spectroscopy. The NC samples were mounted in a titanium sample holder on top of a three-axis piezo-positioner. The sample stage was placed in a homemade optical probe, made of carbon and titanium to minimize possible displacements at high magnetic fields. Laser light was focused on the sample by a singlet lens (10 mm focal length). The same lens was used to collect the PL emission and direct it to the detection setup (Backscattering geometry). The optical probe was mounted inside a liquid helium bath cryostat (4.2 K) inserted in a 50 mm bore Florida-Bitter electromagnet with a maximum field strength of 31 T. All optical experiments were performed in Faraday geometry (light excitation and detection parallel to the magnetic field direction).

For TRPL measurements the excitation was provided by a picosecond pulsed diode-laser operating at 485 nm. The PL signal was detected by an avalanche photo diode connected to a single-photon counter (time-correlated single photon counting). For static, spectrally resolved PL measurements the same excitation source was used but in continuous wave mode. The PL light was guided trough a 300 mm long single grating spectrometer (300 grooves/mm grating) and detected by a liquid nitrogen cooled charge couple device (CCD). Cut-off optical filters were used in excitation and detection, for both PL and TRPL experiments.

For FLN measurements, a very narrow excitation source ($\leq$0.08 nm fwhm) was achieved, using a tunable jet-stream dye (Rhodamine 6G) laser and a 300 mm single grating spectrometer (1200 grooves/mm holographic grating). The output monochromatic beam was collimated with a lens in the optical insert described above. The excitation was circularly polarized with the use of a linear polarizer and a Babinet Soleil compensator. The emitted light was dispersed by a triple-grating Raman spectrometer (subtractive mode). The resonant-PL emission was dispersed by a 500 mm stage (1800 grooves/mm holographic grating) and detected by a liquid nitrogen cooled CCD camera. The emitted photons are detected in crossed and copolarization relative to the laser polarization by using a linear polarizer and a lambda-quarter wave plate.

Conflict of Interest: The authors declare no competing financial interest.

Acknowledgment. The authors thank F. J. P. Wijnen, J. H. Blokland, G. Pettinari and A. Meaney for their help with the FLN experiments and P. T. K Chin for providing some of the CdSe QD samples. We acknowledge the support of HFML-RU/FOM, member of the European Magnetic Field Laboratory (EMFL). Part of this work has been supported by EuroMagNET II under the EU Contract Number 228043.

Supporting Information Available: Additional information including details on the sample characterization and methods, extra optical spectra and a discussion of the acoustic phonon modes of spherical and rod-like nanocrystals. This material is available free of charge *via* the Internet at http://pubs.acs.org.

REFERENCES AND NOTES

1. Klimov, V. I. *Nanocrystal Quantum Dots*, 2nd ed.; CRC Press: Boca Raton, FL, 2010.
2. Efros, A. L.; Rosen, M.; Kuno, M.; Nirmal, M.; Norris, D. J.; Bawendi, M. Band-Edge Exciton in Quantum Dots of Semiconductors with a Degenerate Valence Band: Dark and Bright Exciton States. *Phys. Rev. B: Condens. Matter Mater. Phys.* **1996**, *54*, 4843–4856.
3. Norris, D. J.; Efros, A. L.; Rosen, M.; Bawendi, M. G. Size Dependence of Exciton Fine Structure in CdSe Quantum Dots. *Phys. Rev. B: Condens. Matter Mater. Phys.* **1996**, *53*, 16347–16354.
4. Donegá, C. d. M. Synthesis and Properties of Colloidal Heteronanocrystals. *Chem. Soc. Rev.* **2011**, *40*, 1512–1546.
5. Chin, P. T. K.; de Mello Donegá, C.; van Bavel, S. S.; Meskers, S. C. J.; Sommerdijk, N. A. J. M.; Janssen, R. A. J. Highly Luminescent CdTe/CdSe Colloidal Heteronanocrystals with Temperature-Dependent Emission Color. *J. Am. Chem. Soc.* **2007**, *129*, 14880–14886.
6. Ivanov, S. A.; Piryatinski, A.; Nanda, J.; Tretiak, S.; Zavadil, K. R.; Wallace, W. O.; Werder, D.; Klimov, V. I. Type-II Core/Shell CdS/ZnSe Nanocrystals: Synthesis, Electronic Structures, and Spectroscopic Properties. *J. Am. Chem. Soc.* **2007**, *129*, 11708–11719.
7. de Mello Donegá, C. Formation of Nanoscale Spatially Indirect Excitons: Evolution of the Type-II Optical Character of CdTe/CdSe Heteronanocrystals. *Phys. Rev. B: Condens. Matter Mater. Phys.* **2010**, *81*, 165303.
8. Brovelli, S.; Schaller, R. D.; Crooker, S. A.; García-Santamaría, F.; Chen, Y.; Viswanatha, R.; Hollingsworth, J. A.; Htoon, H.; Klimov, V. I. Nano-Engineered Electron-Hole Exchange Interaction Controls Exciton Dynamics in Core-Shell Semiconductor Nanocrystals. *Nat. Commun.* **2011**, *2*, 280.
9. Rainò, G.; Stöferle, T.; Moreels, I.; Gomes, R.; Kamal, J. S.; Hens, Z.; Mahrt, R. F. Probing the Wave Function Delocalization in CdSe/CdS Dot-in-Rod Nanocrystals by Time- and Temperature-Resolved Spectroscopy. *ACS Nano* **2011**, *5*, 4031–4036.
10. Groeneveld, E.; van Berkum, S.; van Schooneveld, M. M.; Gloter, A.; Meeldijk, J. D.; van den Heuvel, D. J.; Gerritsen, H. C.; de Mello Donegá, C. Highly Luminescent (Zn,Cd)Te/CdSe Colloidal Heteronanowires with Tunable Electron-Hole Overlap. *Nano Lett.* **2012**, *12*, 749–757.
11. Rainò, G.; Stöferle, T.; Moreels, I.; Gomes, R.; Hens, Z.; Mahrt, R. F. Controlling the Exciton Fine Structure Splitting in

CdSe/CdS Dot-in-Rod Nanojunctions. *ACS Nano* **2012**, *6*, 1979–1987.
12. Kim, S.; Fisher, B.; Eisler, H.-J.; Bawendi, M. Type-II Quantum Dots: CdTe/CdSe(Core/Shell) and CdSe/ZnTe(Core/Shell) Heterostructures. *J. Am. Chem. Soc.* **2003**, *125*, 11466–11467.
13. Pandey, A.; Guyot-Sionnest, P. Slow Electron Cooling in Colloidal Quantum Dots. *Science* **2008**, *322*, 929–932.
14. He, J.; Zhong, H.; Scholes, G. D. Electron-Hole Overlap Dictates the Hole Spin Relaxation Rate in Nanocrystal Heterostructures. *Phys. Rev. Lett.* **2010**, *105*, 046601.
15. Hewa-Kasakarage, N. N.; Kirsanova, M.; Nemchinov, A.; Schmall, N.; El-Khoury, P. Z.; Tarnovsky, A. N.; Zamkov, M. Radiative Recombination of Spatially Extended Excitons in (ZnSe/CdS)/CdS Heterostructured Nanorods. *J. Am. Chem. Soc.* **2009**, *131*, 1328–1334.
16. Müller, J.; Lupton, J. M.; Lagoudakis, P. G.; Schindler, F.; Koeppe, R.; Rogach, A. L.; Feldmann, J.; Talapin, D. V.; Weller, H. Wave Function Engineering in Elongated Semiconductor Nanocrystals with Heterogeneous Carrier Confinement. *Nano Lett.* **2005**, *5*, 2044–2049.
17. Crooker, S. A.; Barrick, T.; Hollingsworth, J. A.; Klimov, V. I. Multiple Temperature Regimes of Radiative Decay in CdSe Nanocrystal Quantum Dots: Intrinsic Limits to the Dark-Exciton Lifetime. *Appl. Phys. Lett.* **2003**, *82*, 2793–2795.
18. de Mello Donegá, C.; Bode, M.; Meijerink, A. Size- and Temperature-Dependence of Exciton Lifetimes in CdSe Quantum Dots. *Phys. Rev. B: Condens. Matter Mater. Phys.* **2006**, *74*, 085320.
19. Valerini, D.; Cretí, A.; Lomascolo, M.; Manna, L.; Cingolani, R.; Anni, M. Temperature Dependence of the Photoluminescence Properties of Colloidal CdSe/ZnS Core/Shell Quantum Dots Embedded in a Polystyrene Matrix. *Phys. Rev. B: Condens. Matter Mater. Phys.* **2005**, *71*, 235409.
20. Nirmal, M.; Murray, C. B.; Bawendi, M. G. Fluorescence-Line Narrowing in CdSe Quantum Dots: Surface Localization of the Photogenerated Exciton. *Phys. Rev. B: Condens. Matter Mater. Phys.* **1994**, *50*, 2293–2300.
21. Furis, M.; Htoon, H.; Petruska, M. A.; Klimov, V. I.; Barrick, T.; Crooker, S. A. Bright-Exciton Fine Structure and Anisotropic Exchange in CdSe Nanocrystal Quantum Dots. *Phys. Rev. B: Condens. Matter Mater. Phys.* **2006**, *73*, 241313.
22. Wijnen, F. J. P.; Blokland, J. H.; Chin, P. T. K.; Christianen, P. C. M.; Maan, J. C. Competition between Zero-Phonon and Phonon-Assisted Luminescence in Colloidal CdSe Quantum Dots. *Phys. Rev. B: Condens. Matter Mater. Phys.* **2008**, *78*, 235318.
23. Oron, D.; Aharoni, A.; de Mello Donegá, C.; van Rijssel, J.; Meijerink, A.; Banin, U. Universal Role of Discrete Acoustic Phonons in the Low-Temperature Optical Emission of Colloidal Quantum Dots. *Phys. Rev. Lett.* **2009**, *102*, 177402.
24. Nirmal, M.; Norris, D. J.; Kuno, M.; Bawendi, M. G.; Efros, A. L.; Rosen, M. Observation of the "Dark Exciton" in CdSe Quantum Dots. *Phys. Rev. Lett.* **1995**, *75*, 3728–3731.
25. Califano, M.; Franceschetti, A.; Zunger, A. Temperature Dependence of Excitonic Radiative Decay in CdSe Quantum Dots: The Role of Surface Hole Traps. *Nano Lett.* **2005**, *5*, 2360–2364.
26. Califano, M.; Franceschetti, A.; Zunger, A. Lifetime and Polarization of the Radiative Decay of Excitons, Biexcitons, and Trions in CdSe Nanocrystal Quantum Dots. *Phys. Rev. B: Condens. Matter Mater. Phys.* **2007**, *75*, 115401.
27. Talapin, D. V.; Nelson, J. H.; Shevchenko, E. V.; Aloni, S.; Sadtler, B.; Alivisatos, A. P. Seeded Growth of Highly Luminescent CdSe/CdS Nanoheterostructures with Rod and Tetrapod Morphologies. *Nano Lett.* **2007**, *7*, 2951–2959.
28. Carbone, L.; Nobile, C.; De Giorgi, M.; Sala, F. D.; Morello, G.; Pompa, P.; Hytch, M.; Snoeck, E.; Fiore, A.; Franchini, I. R.; *et al.* Synthesis and Micrometer-Scale Assembly of Colloidal CdSe/CdS Nanorods Prepared by a Seeded Growth Approach. *Nano Lett.* **2007**, *7*, 2942–2950.
29. Pisanello, F.; Martiradonna, L.; Leménager, G.; Spinicelli, P.; Fiore, A.; Manna, L.; Hermier, J.-P.; Cingolani, R.; Giacobino, E.; De Vittorio, M.; *et al.* Room Temperature-Dipolelike Single Photon Source with a Colloidal Dot-in-Rod. *Appl. Phys. Lett.* **2010**, *96*, 033101.
30. Zavelani-Rossi, M.; Lupo, M. G.; Tassone, F.; Manna, L.; Lanzani, G. Suppression of Biexciton Auger Recombination in CdSe/CdS Dot/Rods: Role of the Electronic Structure in the Carrier Dynamics. *Nano Lett.* **2010**, *10*, 3142–3150.
31. Peng, X.; Schlamp, M. C.; Kadavanich, A. V.; Alivisatos, A. P. Epitaxial Growth of Highly Luminescent CdSe/CdS Core/Shell Nanocrystals with Photostability and Electronic Accessibility. *J. Am. Chem. Soc.* **1997**, *119*, 7019–7029.
32. Steiner, D.; Dorfs, D.; Banin, U.; Della Sala, F.; Manna, L.; Millo, O. Determination of Band Offsets in Heterostructured Colloidal Nanorods Using Scanning Tunneling Spectroscopy. *Nano Lett.* **2008**, *8*, 2954–2958.
33. Pietra, F.; Rabouw, F. T.; Evers, W. H.; Byelov, D. V.; Petukhov, A. V.; de Mello Donegá, C.; Vanmaekelbergh, D. Semiconductor Nanorod Self-Assembly at the Liquid/Air Interface Studied by *In Situ* GISAXS and *Ex Situ* TEM. *Nano Lett.* **2012**, *12*, 5515–5523.
34. Zanella, M.; Gomes, R.; Povia, M.; Giannini, C.; Zhang, Y.; Riskin, A.; Van Bael, M.; Hens, Z.; Manna, L. Self-Assembled Multilayers of Vertically Aligned Semiconductor Nanorods on Device-Scale Areas. *Adv. Mater.* **2011**, *23*, 2205–2209.
35. Arora, A. K.; Ramdas, A. K. Resonance Raman Scattering from Defects in CdSe. *Phys. Rev. B: Condens. Matter Mater. Phys.* **1987**, *35*, 4345–4350.
36. García-Santamaría, F.; Brovelli, S.; Viswanatha, R.; Hollingsworth, J. A.; Htoon, H.; Crooker, S. A.; Klimov, V. I. Breakdown of Volume Scaling in Auger Recombination in CdSe/CdS Heteronanocrystals: The Role of the Core-Shell Interface. *Nano Lett.* **2011**, *11*, 687–693.
37. Babinski, A.; Potemski, M.; Christianen, P. C. M. Optical Spectroscopy on Semiconductor Quantum Dots in High Magnetic Fields. *C. R. Phys.* **2013**, *14*, 121.
38. Htoon, H.; Crooker, S. A.; Furis, M.; Jeong, S.; Efros, A. L.; Klimov, V. I. Anomalous Circular Polarization of Photoluminescence Spectra of Individual CdSe Nanocrystals in an Applied Magnetic Field. *Phys. Rev. Lett.* **2009**, *102*, 017402.
39. Goupalov, S. V. Anomalous Polarization of the Photoluminescence from Anisotropic Colloidal CdSe Nanocrystals Subject to External Magnetic Fields. *Phys. Rev. B: Condens. Matter Mater. Phys.* **2009**, *79*, 233301.
40. Blokland, J. H.; Claessen, V. I.; Wijnen, F. J. P.; Groeneveld, E.; de Mello Donegá, C.; Vanmaekelbergh, D.; Meijerink, A.; Maan, J. C.; Christianen, P. C. M. Exciton Lifetimes of CdTe Nanocrystal Quantum Dots in High Magnetic Fields. *Phys. Rev. B: Condens. Matter Mater. Phys.* **2011**, *83*, 035304.
41. Furis, M.; Hollingsworth, J. A.; Klimov, V. I.; Crooker, S. A. Time- and Polarization-Resolved Optical Spectroscopy of Colloidal CdSe Nanocrystal Quantum Dots in High Magnetic Fields. *J. Phys. Chem. B* **2005**, *109*, 15332–15338.
42. Biadala, L.; Louyer, Y.; Tamarat, P.; Lounis, B. Band-Edge Exciton Fine Structure of Single CdSe/ZnS Nanocrystals in External Magnetic Fields. *Phys. Rev. Lett.* **2010**, *105*, 157402.
43. Woggon, U.; Gindele, F.; Wind, O.; Klingshirn, C. Exchange Interaction and Phonon Confinement in CdSe Quantum Dots. *Phys. Rev. B: Condens. Matter Mater. Phys.* **1996**, *54*, 1506–1509.
44. Takagahara, T. Electron-Phonon Interactions in Semiconductor Nanocrystals. *J. Lumin.* **1996**, *70*, 129–143.
45. Tanaka, A.; Onari, S.; Arai, T. Low-Frequency Raman Scattering from CdS Microcrystals Embedded in a Germanium Dioxide Glass Matrix. *Phys. Rev. B: Condens. Matter Mater. Phys.* **1993**, *47*, 1237–1243.
46. Sirenko, A. A.; Belitsky, V. I.; Ruf, T.; Cardona, M.; Ekimov, A. I.; Trallero-Giner, C. Spin-Flip and Acoustic-Phonon Raman Scattering in CdS Nanocrystals. *Phys. Rev. B: Condens. Matter Mater. Phys.* **1998**, *58*, 2077–2087.
47. Saviot, L.; Champagnon, B.; Duval, E.; Kudriavtsev, I.; Ekimov, A. Size Dependence of Acoustic and Optical Vibrational Modes of CdSe Nanocrystals in Glasses. *J. Non-Cryst. Solids* **1996**, *197*, 238–246.
48. Yadav, H. K.; Gupta, V.; Sreenivas, K.; Singh, S. P.; Sundarakannan, B.; Katiyar, R. S. Low Frequency Raman Scattering from Acoustic Phonons Confined in ZnO Nanoparticles. *Phys. Rev. Lett.* **2006**, *97*, 085502.

49. Krauss, T. D.; Wise, F. W. Coherent Acoustic Phonons in a Semiconductor Quantum Dot. *Phys. Rev. Lett.* **1997**, *79*, 5102–5105.
50. Cerullo, G.; De Silvestri, S.; Banin, U. Size-Dependent Dynamics of Coherent Acoustic Phonons in Nanocrystal Quantum Dots. *Phys. Rev. B: Condens. Matter Mater. Phys.* **1999**, *60*, 1928–1932.
51. Sagar, D. M.; Cooney, R. R.; Sewall, S. L.; Dias, E. A.; Barsan, M. M.; Butler, I. S.; Kambhampati, P. Size Dependent, State-Resolved Studies of Exciton-Phonon Couplings in Strongly Confined Semiconductor Quantum Dots. *Phys. Rev. B: Condens. Matter Mater. Phys.* **2008**, *77*, 235321.
52. Palinginis, P.; Tavenner, S.; Lonergan, M.; Wang, H. Spectral Hole Burning and Zero Phonon Linewidth in Semiconductor Nanocrystals. *Phys. Rev. B: Condens. Matter Mater. Phys.* **2003**, *67*, 201307.
53. Biadala, L.; Louyer, Y.; Tamarat, P.; Lounis, B. Direct Observation of the Two Lowest Exciton Zero-Phonon Lines in Single CdSe/ZnS Nanocrystals. *Phys. Rev. Lett.* **2009**, *103*, 037404.
54. Wong, C. Y.; Kim, J.; Nair, P. S.; Nagy, M. C.; Scholes, G. D. Relaxation in the Exciton Fine Structure of Semiconductor Nanocrystals. *J. Phys. Chem. C* **2009**, *113*, 795–811.
55. Huxter, V. M.; Scholes, G. D. Acoustic Phonon Strain Induced Mixing of the Fine Structure Levels in Colloidal CdSe Quantum Dots Observed by a Polarization Grating Technique. *J. Chem. Phys.* **2010**, *132*, 104506.
56. de Mello Donegá, C.; Koole, R. Size Dependence of the Spontaneous Emission Rate and Absorption Cross Section of CdSe and CdTe Quantum Dots. *J. Phys. Chem. C* **2009**, *113*, 6511–6520.
57. Lavallard, P.; Chamarro, M.; Pérez-Conde, J.; Bhattacharjee, A.; Goupalov, S.; Lipovskii, A. Exchange Interaction and Acoustical Phonon Modes in CdTe Nanocrystals. *Solid State Commun.* **2003**, *127*, 439–442.
58. Wei, S.-H.; Zhang, S. B.; Zunger, A. First-Principles Calculation of Band Offsets, Optical Bowings, and Defects in CdS, CdSe, CdTe, and their Alloys. *J. Appl. Phys.* **2000**, *87*, 1304–1311.
59. Zhao, Q.; Graf, P. A.; Jones, W. B.; Franceschetti, A.; Li, J.; Wang; Kim, K. Shape Dependence of Band-Edge Exciton Fine Structure in CdSe Nanocrystals. *Nano Lett.* **2007**, *7*, 3274–3280.
60. Le Thomas, N.; Herz, E.; Schöps, O.; Woggon, U.; Artemyev, M. V. Exciton Fine Structure in Single CdSe Nanorods. *Phys. Rev. Lett.* **2005**, *94*, 016803.
61. Fujii, M.; Nagareda, T.; Hayashi, S.; Yamamoto, K. Low-frequency Raman Scattering from Small Silver Particles Embedded in SiO_2 Thin Films. *Phys. Rev. B: Condens. Matter Mater. Phys.* **1991**, *44*, 6243–6248.
62. Saviot, L.; Champagnon, B.; Duval, E.; Ekimov, A. I. Size-Selective Resonant Raman Scattering in CdS Doped Glasses. *Phys. Rev. B: Condens. Matter Mater. Phys.* **1998**, *57*, 341–346.
63. Salvador, M. R.; Graham, M. W.; Scholes, G. D. Exciton-Phonon Coupling and Disorder in the Excited States of CdSe Colloidal Quantum Dots. *J. Chem. Phys.* **2006**, *125*, 184709.
64. Alvarez, L.; Righi, A.; Guillard, T.; Rols, S.; Anglaret, E.; Laplaze, D.; Sauvajol, J.-L. Resonant Raman Study of the Structure and Electronic Properties of Single-Wall Carbon Nanotubes. *J. Chem. Phys. Lett.* **2000**, *316*, 186–190.
65. Lange, H.; Mohr, M.; Artemyev, M.; Woggon, U.; Thomsen, C. Direct Observation of the Radial Breathing Mode in CdSe Nanorods. *Nano Lett.* **2008**, *8*, 4614–4617.
66. Thonhauser, T.; Mahan, G. D. Predicted Raman Spectra of Si[111] Nanowires. *Phys. Rev. B: Condens. Matter Mater. Phys.* **2005**, *71*, 081307.
67. Efros, A. L. Luminescence Polarization of CdSe Microcrystals. *Phys. Rev. B: Condens. Matter Mater. Phys.* **1992**, *46*, 7448–7458.
68. Hu, M.; Wang, X.; Hartland, G. V.; Mulvaney, P.; Juste, J. P.; Sader, J. E. Vibrational Response of Nanorods to Ultrafast Laser Induced Heating: Theoretical and Experimental Analysis. *J. Am. Chem. Soc.* **2003**, *125*, 14925–14933.
69. de Mello Donegá, C.; Hickey, S. G.; Wuister, S. F.; Vanmaekelbergh, D.; Meijerink, A. Single-Step Synthesis to Control the Photoluminescence Quantum Yield and Size Dispersion of CdSe Nanocrystals. *J. Phys. Chem. B* **2003**, *107*, 489–496.